Fuel 333 (2023) 126211

Contents lists available at ScienceDirect

Fuel

journal homepage: www.elsevier.com/locate/fuel

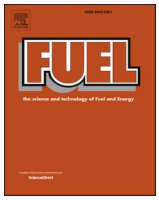

Full Length Article

A six-lump kinetic model for HDPE/VGO blend hydrocracking

Francisco J. Vela [a], Roberto Palos [a,b], David Trueba [a], Tomás Cordero-Lanzac [a,1], Javier Bilbao [a], José M. Arandes [a], Alazne Gutiérrez [a,*]

[a] Department of Chemical Engineering, University of the Basque Country UPV/EHU, PO Box 644, 48080 Bilbao, Spain
[b] Department of Chemical and Environmental Engineering, University of the Basque Country UPV/EHU, Plaza Ingeniero Torres Quevedo 1, 48013 Bilbao, Spain

ARTICLE INFO

Keywords:
Kinetic modeling
Hydrocracking
Plastics
Heavy oil
Fuel
Catalyst deactivation

ABSTRACT

A six lump-based kinetic model has been developed for the hydrocracking of high-density polyethylene (HDPE) blended with vacuum gas oil (VGO) over a PtPd/HY zeolite catalyst. The blend (20 wt% HDPE and 80 wt% VGO) has been hydrocracked in a semi-continuous stirred tank reactor under the following conditions: 400–440 °C; 80 H_2 bar; catalyst to feed (C/F) weight ratio, 0.05–0.1 $g_{cat}\ g_{feed}^{-1}$; reaction time, 15–120 min; and stirring rate, 1300 rpm. The kinetic model, which is an approach to tackle the complex reaction mechanism behind the hydrocracking of a HDPE/VGO blend, predicts the evolution over time of product distribution (gas, naphtha, light cycle oil (LCO), heavy cycle oil (HCO), HDPE and coke). The kinetic model and its computed parameters have been used for the simulation of the HDPE/VGO hydrocracking establishing that a C/F ratio of 0.075 $g_{cat}\ g_{feed}^{-1}$ and temperature–time combinations of 430 °C–10 min and 440 °C–70 min are the optimal operating conditions. Under these conditions, a proper balance between the HCO conversion (>80 %), HDPE conversion (>60 %) and liquid fuel production index (>1.0) would be obtained. This kinetic model could serve as a basis for scaling-up in the valorization of waste plastics by co-feeding them to industrial hydrocracking units, within a Waste-Refinery strategy.

1. Introduction

Hydrocracking is a well-established technology in the oil refining industry for the valorization of heavy and refractory refinery streams, e.g. vacuum resid (VR) and vacuum gas oil (VGO) [1]. The aim of this technology is to convert these unwieldy streams into finished petroleum products, especially motor fuels (gasoline and diesel) that meet established regulations and the specifications for acceptable engine performance [2]. Furthermore, the necessity for drastically reducing CO_2 emissions and the incentives for recycling policies (Circular Economy) trigger an increasing interest for hydrocracking alternative streams to petroleum-derived ones. Among them, do stand out vegetable oils [3], biomass pyrolysis oils [4] and wastes from the consumers society, such as waste plastics [5] and end-of-life tires [6].

Valle et al. [7] for the valorization of biomass and its pyrolysis liquid product (bio-oil) and Palos et al. [8] for the valorization of waste plastics, end-of-life tires and their pyrolysis oils, have stressed out the advantages of integrating the initiatives for upgrading these waste within the structure of conventional oil refineries, converting them into Bio- and Waste-Refineries, respectively. This strategy would use the reaction, separation and reforming units already available in oil refineries, which have a high technological development and are usually already depreciated units. In this way, the integration of the waste valorization in oil refineries would avoid the capital costs that the *ad hoc* units entail, easing at the same time the commercialization of fuels with the composition defined by legal regulations by using the common distribution channels. Moreover, notable savings will be achieved in terms of crude oil consumption, mainly in the recovery of waste plastic and end-of-life tires.

Based on the high capacity of commercial refinery units [9], the co-feeding of a moderate amount of waste plastics together with the benchmark feeds would be enough for avoiding the current severe environmental issues derived from their mismanagement [10]. Furthermore, waste plastics do not commonly content the impurities (S, N and metals) that contribute to deactivate the hydrocracking catalysts [11]. Palos et al. [8] discussed the difficulties to implement these initiatives of plastics valorization in a refinery and the integration of petroleum industry into the circular economy.

Between the different alternative routes [12–14], the hydrocracking

* Corresponding author.
E-mail address: alazne.gutierrez@ehu.eus (A. Gutiérrez).
[1] Present address: SMN Centre for Materials Science and Nanotechnology, Department of Chemistry, University of Oslo, N-0315 Oslo, Norway.

https://doi.org/10.1016/j.fuel.2022.126211
Received 28 July 2022; Received in revised form 29 September 2022; Accepted 2 October 2022
Available online 21 October 2022

Nomenclature

Abbreviations

C/F	catalyst to feed weight ratio
CSTR	continuous stirred tank reactor
HCO	heavy cycle oil
HDPE	high-density polyethylene
LCO	light cycle oil
LDPE	light-density polyethylene
SARA	saturates, aromatics, resins and asphaltenes
TPO	temperature-programmed oxidation
VGO	vacuum gas oil
VR	vacuum resid

Symbols

E	apparent activation energy (kJ/mol)
i	certain lump
j	certain reaction
k	kinetic parameter (h^{-1} g_{cat}^{-1})
k_d	catalyst deactivation kinetic parameter (h^{-1})
m	deactivation order
n_l	number of lumps in the kinetic scheme
n_t	number of experiments
OF	objective function
R	universal gas constant (8.314 J mol^{-1} K^{-1})
t	reaction time (h)
T	reaction temperature (°C) (K in the model)
T*	reference temperature (420 °C) (693.15 K in the model)
w_{HCO}	mass of HCO lump (g)
w_{HDPE}	mass of HDPE (g)
W	total weight of feed (g)
X	conversion (%)
Y	mass fraction

Greek symbols

ψ	deactivation function
ω	weight factor

of polyolefin waste plastics on a bifunctional catalyst is considered as an ideal route for the production of fuels [15,16]. This fact is based on the high versatility and low energy demand of the hydrocracking technology. Moreover, the prospect of having H_2 produced from renewable sources (green hydrogen) increases the potential of the hydrocracking route [17]. Nevertheless, for making the industrial hydrocracking of waste plastics come true, the production of solid results at laboratory- and bench-scale is compulsory to establish the appropriate catalysts and optimal operating conditions. Thus, Karagöz et al. [18] studied the hydrocracking of light-density polyethylene (LDPE) together with VGO using activated carbon-supported Co, Ni and Mo catalysts. They obtained a liquid product with a lower content of aromatics and higher of isoparaffins than that obtained in a cracking stage using an HZSM-5 catalyst. In a previous work [19], we found that the use of a PtPd/HY catalyst in the hydrocracking of a blend of high density polyethylene (HDPE) and VGO (20/80 in mass) increased the conversion of the VGO and the yield and quality of the produced naphtha fraction. In particular, operating at 400 °C under a H_2 pressure of 80 bar, the yield of naphtha obtained was of 31.8 wt%, which was more aromatic than that obtained with the VGO under the same conditions.

Given the effect that the operating conditions have on the product distribution in the hydrocracking processes, it is imperative to have kinetic models for the design and simulation of the hydrocracking reactors. These models could be used for optimizing the operating conditions of the already available units, for the revamping of the outdated industrial units and for the design of *ad hoc* hydrocracking facilities for treating the aforementioned alternative streams. The kinetic modeling of the hydrocracking of heavy refinery streams has evolved using results commonly obtained with slurry-phase catalysts and using batch reactors [20]. The kinetic models proposed in the literature for these feeds are usually lump-based models [21–26], the handling of which for reactor design purposes is by far simpler than those models that consider the reactions of the individual components [27,28]. The lumps are generally established according to the boiling temperature of the components, in order to quantify the yield of gases (dry gas and liquefied petroleum gases), of the liquid products (heavy cycle oil, light cycle oil and naphtha) and of coke (carbonaceous material deposited on the catalyst). Ancheyta et al. [29,30] established lump-based kinetic models considering SARA components (saturates, aromatics, resins and asphaltenes) for the hydrocracking of heavy oil, hence accounting for the composition of the products. These authors also combined a model based on distillation curves with another one based on the SARA components, gas and coke composition [31]. Recently, they have discussed the different kinetic models reported in the literature for the hydrocracking of heavy oil [32]. Furthermore, given the importance of catalyst deactivation in hydrocracking processes, the deactivation kinetics is of special interest. This kinetics is established by means of empirical expressions that quantify the deposition of coke or the simultaneous deposition of coke and metals [33].

As a precedent in the literature about the kinetic modeling of the hydrocracking of plastics, Bin Jumah et al. [34] proposed for the hydrocracking of LDPE over a Pt/Hbeta catalyst a simple 4-lump reaction scheme (LDPE, heavy liquid, naphtha, and gases). They highlighted that the rate-limiting stage, i.e. that with the highest apparent activation energy, was the conversion of the LDPE into heavy liquid based on the diffusion restrictions suffered by the plastic macromolecules. In the current work, the kinetic modeling of the joint hydrocracking of HDPE and VGO using a PtPd/HY catalyst has been studied. The main aim of the work has been to establish an original kinetic model useful for simulating the hydrocracking of the HDPE/VGO blend at a larger scale. With this purpose, they have been quantified in the proposed kinetic model the following lumps: gases, naphtha, light cycle oil (LCO), heavy cycle oil (HCO), HDPE and coke. This distribution is in line with that commonly used in oil refineries for grouping the hydrocarbons produced in the catalytic cracking and hydrocracking processes. In addition, catalyst deactivation by coke deposition has been also considered and quantified in the model, based on its relevance in the results and in the strategy for operating at a larger scale. The kinetic model has been used to predict the effect of the operating conditions, determining the temperature and reaction time values appropriate for achieving great conversions and high yields of fuel.

2. Materials and methods

2.1. Feeds

A high-density polyethylene (HDPE) with an average particle size of 400 μm purchased from Dow Chemical (Tarragona, Spain) was used in this work. Prior to the hydrocracking tests, the HDPE was milled to dust at cryogenic temperatures to avoid the formation of large plastic aggregates. The supplier provided the main physicochemical properties of the HDPE, which were a density of 0.94 g cm^{-3} and a molecular weight of 46.2 kg mol^{-1}.

The vacuum gas oil (VGO) was supplied by Petronor refinery (Muskiz, Biscay, Spain). It consisted on the product stream of a hydrodesulfurization unit which justifies its low contents of S and *N*-

containing compounds (Table S1). The other properties of the VGO are also summarized in Table S1 in the Supplementary Material. A detailed explanation of the methods and procedures followed for characterizing the VGO can be found elsewhere [35]. Shortly, it is a refinery stream with a density of 0.89 g cm^{-3} and a boiling point range of 314–519 °C.

2.2. Catalyst

A PtPd catalyst supported on a HY zeolite with a nominal content for each metal of 1 and 0.5 wt%, respectively, was synthesized via ion-exchange using an already described procedure [36]. The catalyst was intensively characterized by several techniques as it was explained in a previous work [19]. The main physicochemical properties of the catalyst are summarized in Table S2. In brief, the used catalyst has a high specific surface area (620 m^2 g^{-1}), with a micropore area of 543 m^2 g^{-1}, measured by nitrogen adsorption–desorption experiments. The total acidity was measured by temperature-programmed desorption of *tert*-butylamine. The obtained TPD profile is shown in Fig. S1 and the estimated total acidity value was 1.69 $mmol_{t\text{-}BA}$ g^{-1}. Based on the pyridine adsorption/IR experiments, the estimated Brønsted/Lewis acid sites ratio was 0.70, suggesting an important concentration of Lewis acid sites.

2.3. Experimental setup

The experimental setup employed for the hydrocracking reactions was a 100 mL semi continuous stirred tank reactor. A more extended description of the setup is available in our previous work [37]. The operating conditions were varied within the following ranges: 400–440 °C; 80 H_2 bar; catalyst to feed weight ratio (C/F), 0.05–0.075–0.1 g_{cat} g_{feed}^{-1}; and reaction time, 15–120 min. Prior to a reaction, the catalyst was activated *ex situ* in a fixed bed rector at 400 °C for 4 h using a stream of H_2 (30 mL min^{-1}) diluted in N_2 (50 mL min^{-1}). The blend used in the hydrocracking runs consisted of a physical mixture at room temperature of the HDPE and VGO using a fixed weight ratio of 1:4 for all the experiments. After adding the feedstock, the desired amount of catalyst was loaded into the reactor at room temperature. Then, once a leak test was performed, the reactor was pressurized to the desired reaction pressure with hydrogen and heated using a heating jacket up to reaction temperature. Once the desired reaction time was reached, the reactor was cooled down with water using an open water system. To ensure the reproducibility of the data, three replicates were performed for each experiment and the values reported correspond to the averages.

2.4. Product analysis

Gaseous, liquid and solid products (coke and degraded HDPE) were obtained in the hydrocracking runs. The gas stream was quantified by weight difference of the reactor between the beginning and the end of the test. The amounts of liquid product and degraded HDPE were obtained through a two-step solvent extraction procedure described in detail in our previous work [19]. Shortly, in the first extraction THF was used as solvent extracting the liquid products from the mixture (i.e. those corresponding to naphtha, LCO and HCO fractions), whereas in the second one degraded HDPE was extracted using xylene as solvent. The corresponding mass was determined as the difference between the solid products obtained after the first extraction and the remaining solid after the second one (which is the spent catalyst).

The liquid product was subjected to a simulated distillation analysis (ASTM D2887 Standard) to divide the liquid product into three different lumps according to their boiling points: naphtha (35–216 °C), light cycle oil (LCO, 216–350 °C) and heavy cycle oil (HCO, > 350 °C). The equipment used was an Agilent Technologies 6890 GC system equipped with a HP-PONA capillary column (length, 10 m; internal diameter, 0.2 mm) and a FID detector.

Finally, temperature-programmed oxidation (TPO) was used to quantify the amount of coke deposited on the spent catalyst in a TA Instruments (TGA Q500) thermobalance.

2.5. Reaction indexes

Different reaction indexes were defined for measuring the conversion of the HCO (the main and heaviest fraction in the VGO that is converted into the lumps of commercial interest) and HDPE, based on their concentration in the reaction medium. Those indices are:

HCO conversion:

$$X_{HCO} = \frac{(w_{HCO})_{initial} - (w_{HCO})_{final}}{(w_{HCO})_{initial}} \cdot 100 \quad (1)$$

where $(w_{HCO})_{initial}$ and $(w_{HCO})_{final}$ are the mass of HCO in the feed and in the liquid product stream, respectively.

HDPE conversion:

$$X_{HDPE} = \frac{(w_{HDPE})_{initial} - (w_{HDPE})_{final}}{(w_{HDPE})_{initial}} \cdot 100 \quad (2)$$

being $(w_{HDPE})_{initial}$ and $(w_{HDPE})_{final}$ the mass of HDPE in the feed and that obtained through the two-step solvent extraction procedure [19], respectively.

In addition, the dimensionless liquid fuel production index has been also defined to assess the formation of the desired product lumps, i.e. naphtha and LCO [38]:

$$\text{Liquid fuel production index} = \frac{Y_{Naphtha} + Y_{LCO}}{Y_{Gas} + Y_{HCO} + Y_{HDPE} + Y_{Coke}} \quad (3)$$

3. Kinetic modeling

To the best of our knowledge, no specific reaction scheme is available in the literature for the hydrocracking of HDPE/VGO blends. Therefore, we have focused on the models available for the hydrocracking of each feed separately. In this way, the kinetic modeling of the VGO has been extensively studied, either by discrete [39–41] or continuous lump models [42,43]; whereas few references about the hydrocracking of plastics are available in the literature [34,44]. Hence, the kinetic models for the hydrocracking of neat VGO [45,46] have been considered as a starting point for modeling the HDPE/VGO blend, since it is mainly composed of VGO (see Section 2.1).

3.1. Reaction scheme

A 6–lump kinetic model and a reaction network of 11 individual steps is proposed to describe the hydrocracking of the HDPE/VGO blend (Fig. 1). Please note that VGO is mainly formed by HCO lump as it was described above (Table S1). The reaction scheme consists of a series–parallel reaction network where all the lumps are hydrocracked in cascade from the heaviest to the lightest lump. In this way, both the HCO and the HDPE lumps can be directly converted into LCO, naphtha and gas; the LCO can produce naphtha and gas; and naphtha can be, in turn, hydrocracked producing gas. Furthermore, the probability of producing coke from molecules within the LCO, naphtha and gas lumps is negligible according to the literature [21,41,46]. Moreover, given the high content of polyaromatic components in the feed (Table S1), the formation of coke was assumed to only come from the HCO lump. This has been considered as a reversible reaction since some poorly developed coke structures can be hydrocracked and converted again into liquid hydrocarbons [39].

3.2. Model equations and methodology

The methodology used for the analysis of the kinetic data was based

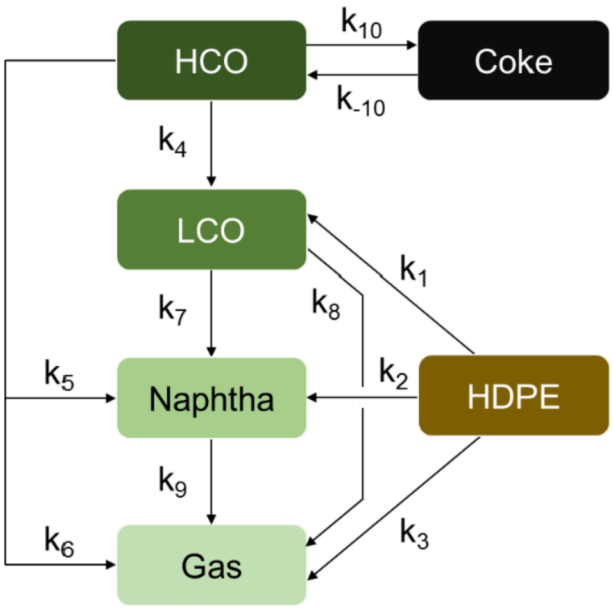

Fig. 1. Proposed reaction network for describing the hydrocracking of the HDPE/VGO blend.

on the recommendations available in the literature for catalytic processes with complex reactions networks in which catalyst deactivation is considered [47–49]. In addition, the following assumptions were made for establishing the equations that define the system: (i) based on the high stirring rate used (1300 rpm) the external diffusion resistance is negligible [29]; (ii) as there will be some intra-particle diffusion resistance, apparent kinetic parameters will be computed; (iii) the concentration of the gas and liquid phases is uniform throughout the reactor (CSTR model) [50]; (iv) there are no temperature gradients [51]; and (v) the pressure is constant in the reaction medium over time, which is caused by the continuous feeding of H_2 that creates an excess of this reactant (semi-continuous model).

Thus, the conservation equations that described the evolution with time of the different pseudo-components proposed in the 6-lump reaction scheme (Fig. 1) are displayed below:

$$\frac{dY_{HDPE}}{dt} = -\Psi\ [(k_1 + k_2 + k_3)\ Y_{HDPE}]\cdot C/F\cdot W \tag{4}$$

$$\frac{dY_{HCO}}{dt} = \Psi\ \left[k_{-10} Y_{Coke} - (k_4 + k_5 + k_6 + k_{10})\ Y_{HCO}^2\right]\cdot C/F\cdot W \tag{5}$$

$$\frac{dY_{LCO}}{dt} = \Psi\ \left[k_1 Y_{HDPE} + k_4 Y_{HCO}^2 - (k_7 + k_8)\ Y_{LCO}\right]\cdot C/F\cdot W \tag{6}$$

$$\frac{dY_{Naphtha}}{dt} = \Psi\ \left[k_2 Y_{HDPE} + k_5 Y_{HCO}^2 + k_7\ Y_{LCO} - k_9\ Y_{Naphtha}\right]\cdot C/F\cdot W \tag{7}$$

$$\frac{dY_{Gas}}{dt} = \Psi\ \left[k_3 Y_{HDPE} + k_6 Y_{HCO}^2 + k_8\ Y_{LCO} + k_9\ Y_{Naphtha}\right]\cdot C/F\cdot W \tag{8}$$

$$\frac{dY_{Coke}}{dt} = \Psi\ \left[k_{10} Y_{HCO}^2 - k_{-10}\ Y_{Coke}\right]\cdot C/F\cdot W \tag{9}$$

where Y_i is the yield of each lump *i*, k_j is the apparent kinetic constant for reaction *j*, C/F is the catalyst to feed weight ratio, W is the total weight of feed (initial feed loading in the batch reactor) and ψ is the deactivation function.

One should note that the hydrocracking of the different lumps has been described by means of first-order irreversible reactions with the exception to those reactions in which the HCO lump has acted as a reactant, which have been assumed as second-order irreversible reactions. This strategy is commonly used in the literature [52–54] because it describes more accurately the different reactivity of the wide variety of heavy compounds comprehended within the HCO lump. In addition, all the kinetic equations are independent of both H_2 partial pressure and stoichiometry coefficients due to the great H_2 excess in the reaction medium [55,56].

The main catalyst deactivation cause would predictably be the deposition of coke, which has been quantified as a product in the kinetic model (Fig. 1). The low concentration of S and N in the VGO (Table S1) and the activity recovery of the catalyst after being submitted to an air combustion process at 550 °C, allow for minimizing the relevance of the poisoning and metal sintering as catalyst deactivation causes. Consequently, the catalyst deactivation function has been defined by means of the following hyperbolic function [57]. The selection of a hyperbolic deactivation function is based on the works of kinetic modeling of hydrocracking systems in batch reactors developed by Martinez and Ancheyta [54], thus maintaining the coherence of the model with their methodology.

$$\Psi = \frac{1}{(1 + k_d\ t)^m} \tag{10}$$

where k_d is the catalyst deactivation kinetic constant and m the deactivation order. Note that it has been considered that all the reactions described in the reaction network are non-selectively affected by catalyst deactivation.

The kinetic constants are defined as temperature-dependent by means of the reparameterized Arrhenius equation:

$$k_j = k_j^*\ \exp\left[-\frac{E_j}{R}\left(\frac{1}{T} - \frac{1}{T^*}\right)\right] \tag{11}$$

being T* the reference temperature (420 °C, central point of our experimental runs), k_j^* the apparent kinetic constant at the reference temperature for each *j* reaction, E_j the apparent activation energy of the *j* reaction and R the universal gas constant. The same expression in Eq. (11) was used to define the dependency of the deactivation kinetic constant (k_d) with temperature.

3.3. Calculation methodology

The parameters of the proposed kinetic model were determined by fitting the values predicted by the model to the experimental data obtained at different reaction times for the ranges of temperatures and C/F ratios studied. In this way, the optimal values of the parameters will be those that minimize the following objective function:

$$OF = \sum_1^{n_t} \sum_1^{n_l} \omega_i\ \left(Y_i^{exp} - Y_i^{calc}\right)^2 \tag{12}$$

where n_t is the total number of experiments (including the repetitions), n_l is the number of lumps and ω_i is the weighting factor for each lump *i*. Furthermore, the superscripts "exp" and "calc" denote the average value experimentally determined and calculated yields, respectively.

The weight factors are calculated with Eq. (13) for each lump [58,59]. Thus, the minority lumps in the reaction medium have a higher weight factor.

$$\omega_i = \frac{1}{\sum_1^{n_l} Y_i^{calc}} \tag{13}$$

For this purpose, an in-house developed MATLAB algorithm has been used. It consists essentially on three iteratively repeated steps: (i) an initial set of kinetic parameters is supplied to solve the system of ordinary differential equations; (ii) the sum of the squared errors is calculated; and (iii) this error is minimized to obtain the optimal values of the kinetic constants.

In order to ease the resolution, the sequential method proposed by

Ancheyta-Juárez and Sotelo-Bovás [60] was applied to estimate rate constants. In this way, the optimization was carried out in successive stages. The used kinetic networks for the sequential method are the same proposed by these authors [60] and are detailed in Fig. S2, with reaction networks progressively more complex and using the optimal parameters of each model as initial guess values of the estimates of the next model constants. This process was repeated until ending in the model corresponding to the reaction network described in Fig. 1.

4. Results and discussion

4.1. Fitting and validation of the kinetic model

The values of the apparent kinetic parameters at the reference temperature (420 °C) and of the apparent activation energies for the kinetic model corresponding to reaction network in Fig. 1 are displayed in Table 1. Furthermore, these parameters were used to reproduce the evolution of the product yields with the extent of the reaction time for the tested values of C/F (0.05, 0.075 and 0.1 $g_{cat}\ g_{feed}^{-1}$) and temperature (400, 420 and 440 °C). The results obtained have been depicted in Figs. 2-4. The slight deviation observed at long reaction times and high temperature between the experimental and the model predicted values for the lumps of gas and naphtha could be attributed to experimental errors. Another cause of the deviation for long reaction times can be the limitations of the deactivation kinetics equation (Eq. (10)). The used deactivation model does not consider that the catalyst activity tends to a constant remaining activity value. This suggests the interest in equations that consider this circumstance [61]. In addition, at high temperatures, deviations can be explained by the contribution of thermal cracking. Anyway, overall an acceptable good fitting of the model was obtained as it can be seen in the parity plot of Fig. 5, where the experimental values are represented versus the data predicted by the model.

Regarding the values obtained for the apparent kinetic parameters (Table 1), the importance of the reactions in series is evident from the LCO lump detailed in Fig. 1 (LCO → naphtha → gas). In this way, the apparent kinetic constant for the conversion of LCO to naphtha (k_7) is three orders of magnitude higher than the constant for its direct conversion to gas (k_8). This result reinforces the idea, widely reported in the literature [62], that the conversion of heavy fractions occurs through a cascade mechanism composed of series reactions. Indeed, the HDPE is predicted to be mainly converted following similar reactions in series. The plastic macromolecules are preferably converted into LCO ($k_1 > k_2 > k_3$), that is sequentially converted into naphtha and gas. In fact, the apparent kinetic constant values for the formation of naphtha and gas are significantly lower (one and two orders of magnitude) than that of LCO formation. Therefore, the formation rate of other products rather than LCO from the plastic can be assumed almost negligible. Otherwise, HCO, which is the main and heaviest fraction in the VGO (Table S1), is predicted to be converted into LCO and naphtha with similar apparent kinetic constants ($k_4 \approx k_5$). This result is in line with those reported by Sánchez et al. [45], as they also observed that heavy oil fractions are preferentially and indifferently converted into LCO and naphtha.

The apparent kinetic parameters of the reactions that produced molecules within the LCO lump, from either the HDPE or the HCO lumps (k_1 and k_4, respectively), are lower than the parameters of the reactions in which the LCO is converted to naphtha or gas (k_7 and k_8, respectively). However, the common trend reported in the literature is usually the opposite one, in which the formation of the heavy molecules is preferential [63]. This fact lies on the catalyst used in this work (PtPd/HY), with a high hydrocracking activity that promotes in a large extent the formation of both naphtha and gas (Figs. 4–6). Thus, the lower yields of LCO experimentally observed may be explained by the predicted faster hydrocracking of LCO, formed from the HDPE and HCO lumps, into naphtha. Indeed, the conversion of LCO into naphtha is one of the reactions with the highest apparent kinetic constant from all of those proposed in this model (Table 1).

In concordance with the literature [16,34], the most important reactions in the hydrocracking of neat polyolefins are those that generate LCO and naphtha and, in a lesser extent, the production of gases. This fact is also reflected in our results (Table 1), since the HDPE is predicted to mainly form LCO, which is subsequently converted to lighter fractions. In contrast, the model estimates a slower direct formation of naphtha from the HDPE and a practically negligible production of gases from the HDPE.

Additionally, the character of the LCO as an intermediate in the reaction network has been clearly exposed. Indeed, its conversion to naphtha is by far faster than its production from the HDPE and the HCO lumps ($k_7 > k_1 \approx k_4$, respectively). That is why its yield goes through a maximum for all the operating conditions assessed (Figs. 2-4), as it has been widely reported in the literature [44,64]. On the other hand, the gas fraction seems to be more given to be formed from the naphtha lump (k_9) instead that directly from the HDPE (k_3), HCO (k_6) or LCO (k_8) lumps. In addition, the yield of the gas products increases continuously with the reaction time, especially at the highest C/F ratio (Fig. 4), due to the high hydrocracking activity of the catalyst [65,66].

Catalyst deactivation strongly depends on the reactivity of the soft coke [39]. Indeed, coke lump molecules could condense to heavier polyaromatic structures or, on the contrary, could be hydrogenated again into liquid hydrocarbons. The equilibrium between the aforementioned reactions explains the trend followed by the yield of coke with the extent of reaction time, in which it increases rapidly for short reaction times (15 min) and remains constant from that point on. Thus, at short contact times the adsorption of polyaromatics hydrocarbons on the acid sites of the catalyst is promoted forming a fraction of hard coke that is very stable given its low H/C ratio.

Analyzing the values of the apparent activation energies reported in Table 1, the highest activation energy is found by the formation of the LCO from the HDPE (233 kJ mol^{-1}). All apparent activation energy values are in the range of reaction-limited regime (>63 kJ mol^{-1}) but the lowest one, corresponding to the formation of gas from the naphtha

Table 1
Order, apparent kinetic parameters at the reference temperature and activation energies for the reactions involved in the hydrocracking of the HDPE/VGO blend.

Reaction, kinetic parameter	Order*	k_j (420 °C)	Units	E_j (kJ mol^{-1})
HDPE → LCO, k_1	1	$(3.80 \pm 0.04)\ 10^{-2}$	$h^{-1}\ g_{cat}^{-1}$	233 ± 31
HDPE → Naphtha, k_2	1	$(1.03 \pm 0.16)\ 10^{-3}$	$h^{-1}\ g_{cat}^{-1}$	109 ± 51
HDPE → Gas, k_3	1	$(1.08 \pm 0.03)\ 10^{-4}$	$h^{-1}\ g_{cat}^{-1}$	143 ± 44
HCO → LCO, k_4	2	$(3.72 \pm 0.48)\ 10^{-2}$	$h^{-1}\ g_{cat}^{-1}$	70 ± 10
HCO → Naphtha, k_5	2	$(3.38 \pm 0.40)\ 10^{-2}$	$h^{-1}\ g_{cat}^{-1}$	182 ± 20
HCO → Gas, k_6	2	$(1.20 \pm 0.22)\ 10^{-3}$	$h^{-1}\ g_{cat}^{-1}$	141 ± 31
LCO → Naphtha, k_7	1	$(1.89 \pm 0.23)\ 10^{-1}$	$h^{-1}\ g_{cat}^{-1}$	63 ± 6
LCO → Gas, k_8	1	$(2.58 \pm 0.03)\ 10^{-4}$	$h^{-1}\ g_{cat}^{-1}$	190 ± 10
Naphtha → Gas, k_9	1	$(5.65 \pm 0.51)\ 10^{-1}$	$h^{-1}\ g_{cat}^{-1}$	3 ± 0.8
HCO → Coke, k_{10}	2	$(2.94 \pm 0.39)\ 10^{-3}$	$h^{-1}\ g_{cat}^{-1}$	213 ± 13
Coke → HCO, k_{-10}	1	$(2.59 \pm 0.01)\ 10^{-1}$	$h^{-1}\ g_{cat}^{-1}$	97 ± 5
Deactivation, k_d	0.55	28.1 ± 2.3	h^{-1}	48 ± 10

* Only deactivation order was fitted as reaction orders were already defined in Eqs. 4–9

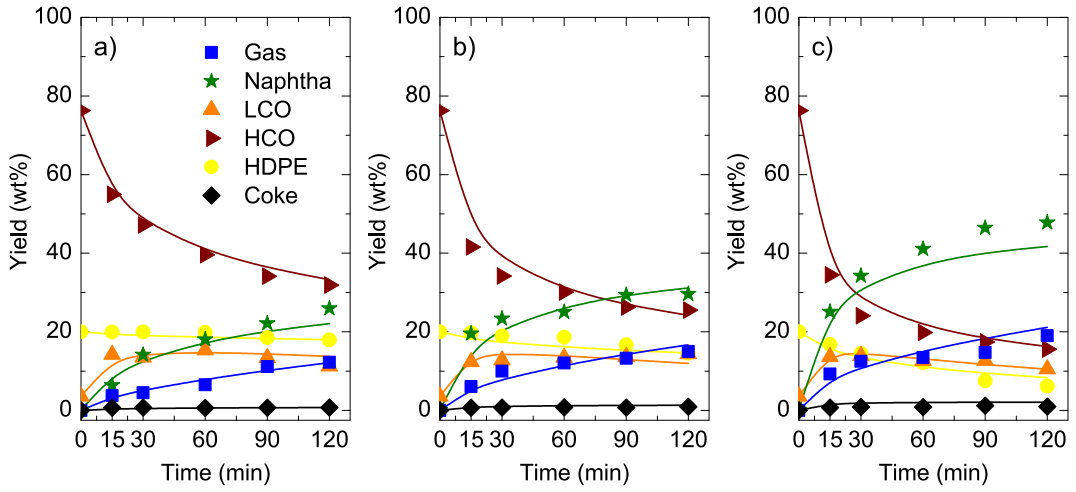

Fig. 2. Evolution of the product yields with the reaction time at 400 (a), 420 (b) and 440 °C (c). (The dots correspond to the experimental data and the lines to the calculated values). Operating conditions: C/F ratio = 0.05 $g_{cat}\ g_{feed}^{-1}$.

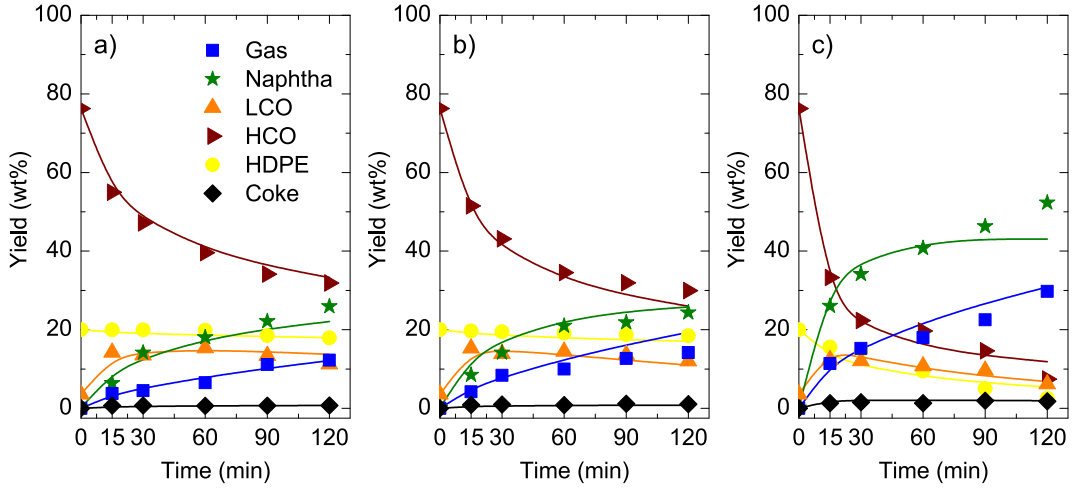

Fig. 3. Evolution of the product yields with the reaction time at 400 (a), 420 (b) and 440 °C (c). (The dots correspond to the experimental data and the lines to the calculated values). Operating conditions: C/F ratio = 0.075 $g_{cat}\ g_{feed}^{-1}$.

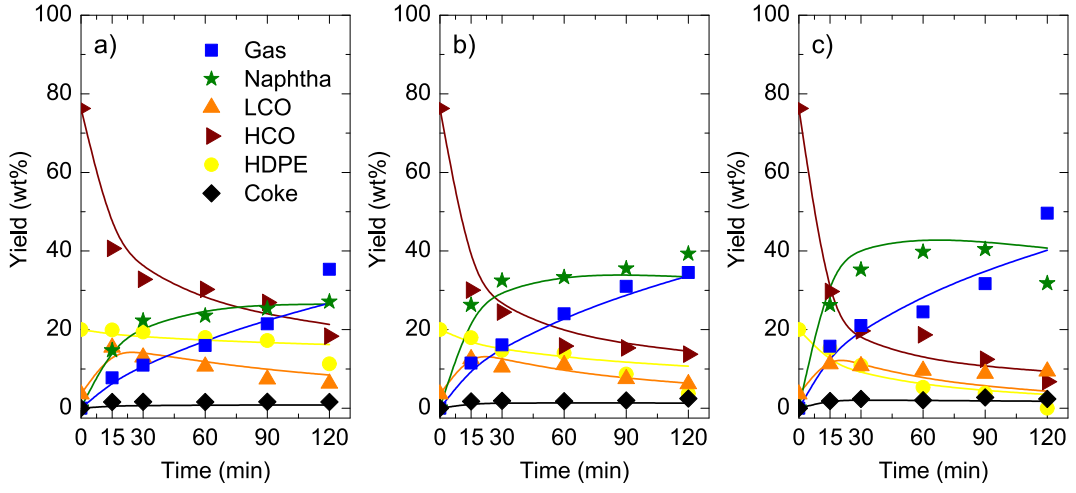

Fig. 4. Evolution of the product yields with the reaction time at 400 (a), 420 (b) and 440 °C (c). (The dots correspond to the experimental data and the lines to the calculated values). Operating conditions: C/F ratio = 0.1 $g_{cat}\ g_{feed}^{-1}$.

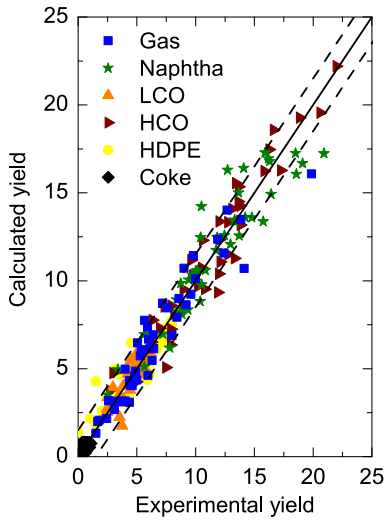

Fig. 5. Parity diagram of lump yield for the proposed hydrocracking kinetic model.

(3 kJ mol^{-1}). This reaction is predicted to be barely affected by temperature at the studied range, which may be due to the high reactivity of hydrocarbons in the naphtha lump to form gas through a thermal route within the 400–440 °C range. In that hypothetical case, this reaction would not be affected by catalyst deactivation (ψ function), which could also explain the highest deviations calculated for k_9. In the literature [52,54], similar apparent activation energy values have been reported for the production of LCO, naphtha and gas from the HCO. Among them (k_4-k_6), the lowest apparent activation energy is computed for the formation of LCO (70 kJ mol^{-1}). In contrast, one of the most elevated apparent activation energy is found for the condensation of HCO towards coke (213 kJ mol^{-1}), slightly higher than that reported by Al-Attas et al. [41] in the hydrocracking of neat VGO. This result exposes the marked effect of the temperature on promoting the condensation of the coke precursors while the hydrogenation of these precursors is disfavored. Moreover, coke was assumed to be formed only from HCO, whereas HDPE only forms LCO, naphtha and gas (Fig. 1). These hypothesis, which provided the best experimental data fitting, agrees with the aromatic/polyaromatics species present in each lump. VGO contains a significant concentration of condensed species [67] that easily form coke that remains retained in the zeolite channels. Otherwise, the dissolved HDPE forms lineal oligomeric chains which quickly become compounds within the LCO lump. Those compounds, most of the time saturated, are not retained in the crystalline channels of the zeolite, and require a much higher temperature than 440 °C to condense and form polyaromatic structures. It should be highlighted that these results for the activation energies are in line with the general trend discussed by Félix et al. [32] in the hydrocracking of different heavy streams. They reported that the activation energy of the conversion stages of heavy fractions are notably minor than those of middle fractions. In this way, it is remarkable the activation energy of the conversion of HDPE molecules into LCO (233 kJ mol^{-1}). A contribution of thermal cracking can also explain these results, with a higher contribution of this route at the highest tested temperature (440 °C).

4.2. Simulation and optimal operating conditions

Using the kinetic model proposed in Section 3.1 and the corresponding calculated kinetic parameters (Table 1), the hydrocracking of the HDPE/VGO blend has been simulated within the proposed ranges of temperature (400–440 °C) and reaction time (0–120 min) for the three C/F ratios (0.05–0.1 $g_{cat}\ g_{feed}^{-1}$). The main aim of these simulations is to determine the operating conditions that maximize the conversion of HCO and HDPE and the liquid fuel production index.

Fig. 6 shows that both the reaction time and temperature favor the conversion of the HCO lump. This effect is more pronounced for the highest C/F ratio (Fig. 6c), achieving higher conversions for the same ranges of operating conditions. In this way, the maximum HCO conversion obtained for a C/F ratio of 0.05 $g_{cat}\ g_{feed}^{-1}$ is ca. 80 % at a temperature of 440 °C and a reaction time of 120 min (Fig. 6a). However, an increase in the C/F ratio to 0.075 $g_{cat}\ g_{feed}^{-1}$ (Fig. 6b) allows to reach conversion levels above 80 % at shorter reaction times (60 min) when operating at 440 °C. Furthermore, this conversion extent can be also obtained at 420 °C but requiring 120 min. Finally, at the highest C/F ratio (0.1 $g_{cat}\ g_{feed}^{-1}$) even less severe operating conditions are required to achieve conversion values above 80 % (Fig. 6c). At temperatures of 420 and 440 °C, 90 and 30 min reaction times are respectively needed to reach this target conversion. Furthermore, the maximum conversion level (88 %) that can be obtained corresponds to the harshest operating conditions (440 °C and 120 min).

With regard to HDPE conversion (Fig. 7), the maximum simulated conversion value calculated at the lowest C/F ratio (0.05 $g_{cat}\ g_{feed}^{-1}$) is of 57.8 % (120 min and 440 °C) as displayed in Fig. 7a. Since this maximum value is relatively poor, an increase in the C/F ratio to 0.075 $g_{cat}\ g_{feed}^{-1}$ (Fig. 7b) allows for obtaining HDPE conversions above 60 % at 440 °C and reaction times above 60 min, with a maximum HDPE conversion of 73 % (440 C, 120 min). A further increase in the C/F ratio up to 0.1 $g_{cat}\ g_{feed}^{-1}$ (Fig. 7c) increases the conversion level up to 70 % for reaction times higher of 60 min and 440 °C, with the maximum HDPE conversion being of 82.5 %. It should be highlighted how temperature-dependent the HDPE conversion is, predicting values below 50 % for any of the C/F ratios or the reaction times when the simulated temperature is

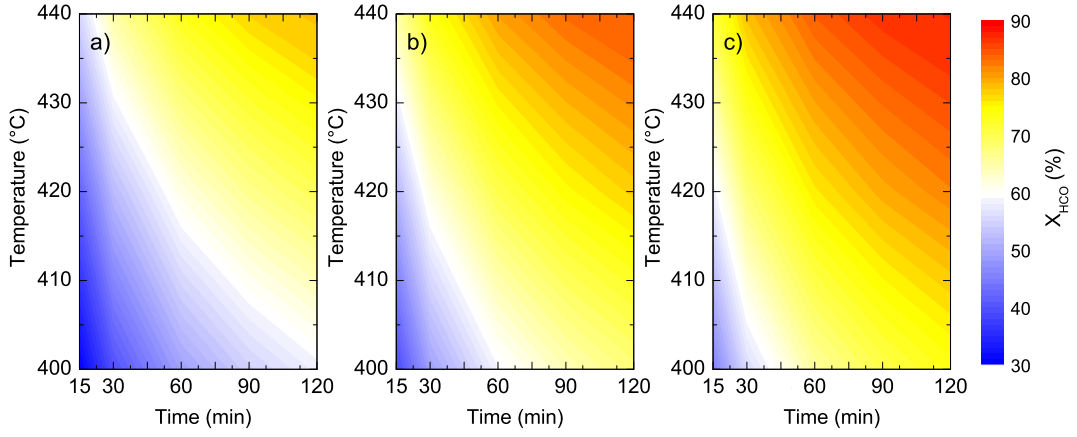

Fig. 6. Contour plot of temperature versus reaction time showing the HCO conversion for a C/F ratio of 0.05 (a), 0.075 (b) and 0.1 $g_{cat}\ g_{feed}^{-1}$ (c).

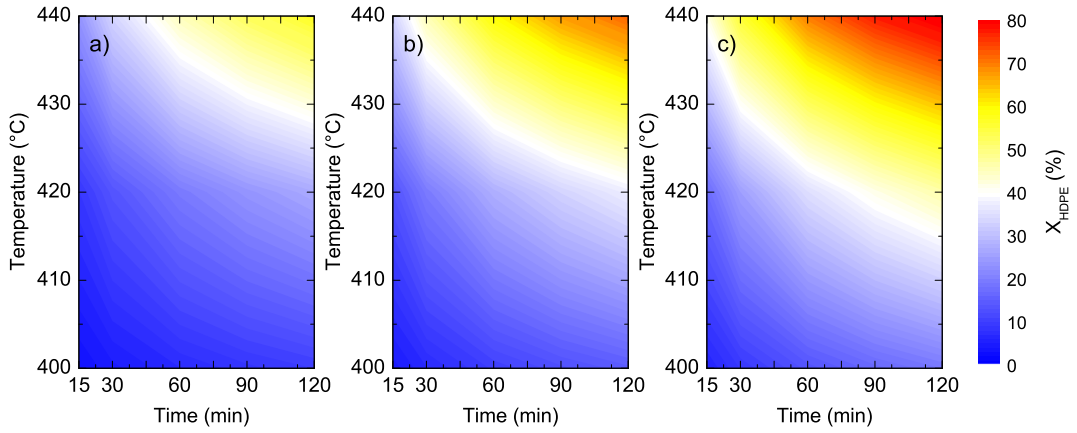

Fig. 7. Contour plot of temperature versus reaction time showing the HDPE conversion for a C/F ratio of 0.05 (a), 0.075 (b) and 0.1 $g_{cat}\ g_{feed}^{-1}$ (c).

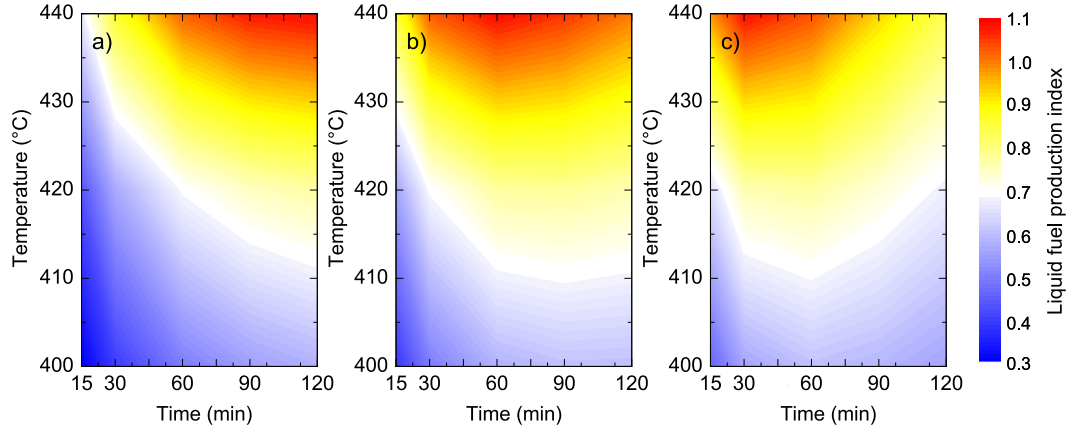

Fig. 8. Contour plot of temperature versus reaction time showing the liquid fuel production index for a C/F ratio of 0.05 (a), 0.075 (b) and 0.1 $g_{cat}\ g_{feed}^{-1}$ (c).

below 420 °C.

The liquid fuel production index shows different behaviors with temperature and reaction time when the C/F ratio is increased (Fig. 8). Therefore, for a C/F ratio of 0.05 $g_{cat}\ g_{feed}^{-1}$ (Fig. 8a), the liquid fuel production index increases with both temperature ad reaction time, obtaining the maximum value of 1.1 at 440 °C and 120 min. However, for C/F ratios of 0.075 and 0.1 $g_{cat}\ g_{feed}^{-1}$ (Fig. 8b and 8c, respectively) the liquid fuel production index increases linearly with temperature but not with reaction time. Thus, the highest value obtained (1.1) is predicted for a C/F ratio of 0.075 $g_{cat}\ g_{feed}^{-1}$ at 440 °C and a reaction time of 60 min, which is displaced towards shorter contact times (30 min) for a C/F ratio of 0.1 $g_{cat}\ g_{feed}^{-1}$.

Based on these results, it can be concluded that the optimal operating conditions for hydrocracking the HDPE/VGO blend within the range of conditions studied are a C/F ratio of 0.075 $g_{cat}\ g_{feed}^{-1}$ and temperature–time combinations of 430 °C-120 min and 440 °C-70 min. These operating conditions would allow to achieve a commitment between the HCO conversion (above 80 %), the HDPE conversion (>60 %) and a liquid fuel production index above 1.

Note that the application of the proposed kinetic model is optimal in the range of conditions and with the feed and catalysts studied. The validation of the model with new catalysts and a wider operating conditions framework would allow to use it under different conditions such as different plastics and catalysts with properties that promote the production of naphtha and attenuate deactivation.

5. Conclusions

A six-lump kinetic model has been established for describing the hydrocracking of a blend of HDPE (20 wt%) and VGO (80 wt%) over a PtPd/HY catalyst. The kinetic model has been developed with the mass conservation equations of the different lumps (gas, naphtha, LCO, HCO, HDPE and coke) and considering a catalyst deactivation kinetics. The model is based on a reaction network of 11 reactions that integrates the conversion of the HDPE with the cascade reactions of the VGO hydrocracking.

The model has fitted the experimental results in a wide range of experimental conditions (catalyst to feed weight ratio, temperature and reaction time) and the kinetic parameters (apparent kinetic constants and apparent activation energies) have been explained according to the different reactivity of the lumps and in concordance with the literature. The high catalyst activity is appropriate for the selective production of naphtha, the formation of which from the LCO lump (main product obtained from the hydrocracking of the HDPE) is one of the stages with the highest apparent kinetic constant and lowest apparent activation energy.

From the experimental results and the kinetic model predictions, the optimal operating conditions are a C/F ratio of 0.075 $g_{cat}\ g_{feed}^{-1}$ and temperature–time combinations of 430 °C-120 min or 440 °C-70 min. These operating conditions allow for achieving a good commitment between the HCO and the HDPE conversions (above 80 and 60 %, respectively) and a liquid fuel production index above than 1.

However, it could be a useful tool for studying the hydrocracking of other HDPE contents and other combinations of waste plastics and VGO (or other secondary refinery streams). Thereby, it would help the growing evolution and scale-up of the Waste-Refinery strategy, involving oil refineries within the recycling chain of waste from the consumers society.

CRediT authorship contribution statement

Francisco J. Vela: Investigation, Formal analysis, Writing – original draft. **Roberto Palos:** Writing – review & editing, Visualization, Conceptualization. **David Trueba:** Formal analysis, Software. **Tomás Cordero-Lanzac:** Software, Writing – review & editing. **Javier Bilbao:** Writing – review & editing, Supervision, Project administration, Funding acquisition. **José M. Arandes:** Resources, Project administration, Funding acquisition. **Alazne Gutiérrez:** Writing – original draft, Supervision, Methodology, Visualization.

Declaration of Competing Interest

The authors declare that they have no known competing financial interests or personal relationships that could have appeared to influence the work reported in this paper.

Data availability

Data used for the kinetic modelling are shown in the paper

Acknowledgments

This work has been carried out with the financial support of the Ministry of Science, Innovation and Universities (MICIU) of the Spanish Government (grant RTI2018-096981-B-I00), the European Union's ERDF funds and Horizon 2020 research and innovation program under the Marie Skłodowska-Curie Actions (grant No 823745) and the Basque Government (grant IT1645-22). David Trueba thanks the University of the Basque Country UPV/EHU for his PhD grant (PIF 2018).

The authors acknowledge Petronor refinery for providing the feed used in the work.

Appendix A. Supplementary data

Supplementary data to this article can be found online at https://doi.org/10.1016/j.fuel.2022.126211.

References

[1] Thybaut JW, Marin GB. Multiscale aspects in hydrocracking: from reaction mechanism over catalysts to kinetics and industrial application. Adv Catal 2016;59:109–238. https://doi.org/10.1016/bs.acat.2016.10.001.
[2] Marafi A, Albazzaz H, Rana MS. Hydroprocessing of heavy residual oil: Opportunities and challenges. Catal Today 2019;329:125–34. https://doi.org/10.1016/J.CATTOD.2018.10.067.
[3] Tirado A, Ancheyta J. Scaling up the performance of a reactor model for hydrotreating vegetable oil from bench-scale to pilot-scale reactors. Ind Eng Chem Res 2020;59:21712–9. https://doi.org/10.1021/acs.iecr.0c04538.
[4] Cordero-Lanzac T, Rodríguez-Mirasol J, Cordero T, Bilbao J. Advances and challenges in the valorization of bio-oil: hydrodeoxygenation using carbon-supported catalysts. Energy Fuels 2021;35:17008–31. https://doi.org/10.1021/acs.energyfuels.1c01700.
[5] Trueba D, Palos R, Bilbao J, Arandes JM, Gutiérrez A. Product composition and coke deposition in the hydrocracking of polystyrene blended with vacuum gasoil. Fuel Process Technol 2021;224:107010. https://doi.org/10.1016/j.fuproc.2021.107010.
[6] Palos R, Kekäläinen T, Duodu F, Gutiérrez A, Arandes JM, Jänis J, et al. Detailed nature of tire pyrolysis oil blended with light cycle oil and its hydroprocessed products using a NiW/HY catalyst. Waste Manag 2021;128:36–44. https://doi.org/10.1016/j.wasman.2021.04.041.
[7] Valle B, Remiro A, García-Gómez N, Gayubo AG, Bilbao J. Recent research progress on bio-oil conversion into bio-fuels and raw chemicals: a review. J Chem Technol Biotechnol 2019;94:670–89. https://doi.org/10.1002/JCTB.5758.
[8] Palos R, Gutiérrez A, Vela FJ, Olazar M, Arandes JM, Bilbao J. Waste Refinery: the valorization of waste plastics and end-of-life tires in refinery units. A review. Energy Fuels 2021;35:3529–57. https://doi.org/10.1021/acs.energyfuels.0c03918.
[9] Ruble I, The US. crude oil refining industry: recent developments, upcoming challenges and prospects for exports. J Econ Asymmetries 2019;20:e00132.
[10] Gangadoo S, Owen S, Rajapaksha P, Plaisted K, Cheeseman S, Haddara H, et al. Nano-plastics and their analytical characterisation and fate in the marine environment: From source to sea. Sci Total Environ 2020;732:138792. https://doi.org/10.1016/j.scitotenv.2020.138792.
[11] Marafi M, Furimsky E. Hydroprocessing catalysts containing noble metals: deactivation, regeneration, metals reclamation, and environment and safety. Energy Fuels 2017;31:5711–50. https://doi.org/10.1021/acs.energyfuels.7b00471.
[12] Huang J, Veksha A, Chan WP, Giannis A, Lisak G. Chemical recycling of plastic waste for sustainable material management: a prospective review on catalysts and processes. Renew Sustain Energy Rev 2022;154:111866. https://doi.org/10.1016/j.rser.2021.111866.
[13] Jahirul MI, Rasul MG, Schaller D, Khan MMK, Hasan MM, Hazrat MA. Transport fuel from waste plastics pyrolysis – a review on technologies, challenges and opportunities. Energy Convers Manag 2022;258:115451. https://doi.org/10.1016/j.enconman.2022.115451.
[14] Li N, Liu H, Cheng Z, Yan B, Chen G, Wang S. Conversion of plastic waste into fuels: a critical review. J Hazard Mater 2022;424:127460. https://doi.org/10.1016/j.jhazmat.2021.127460.
[15] Munir D, Irfan MF, Usman MR. Hydrocracking of virgin and waste plastics: A detailed review. Renew Sustain Energy Rev 2018;90:490–515. https://doi.org/10.1016/j.rser.2018.03.034.
[16] Mangesh VL, Tamizhdurai P, Santhana Krishnan P, Narayanan S, Umasankar S, Padmanabhan S, et al. Green energy: Hydroprocessing waste polypropylene to produce transport fuel. J Clean Prod 2020;276:124200. https://doi.org/10.1016/j.jclepro.2020.124200.
[17] Kots PA, Vance BC, Vlachos DG. Polyolefin plastic waste hydroconversion to fuels, lubricants, and waxes: a comparative study. React Chem Eng 2022;7:41–54. https://doi.org/10.1039/d1re00447f.
[18] Karagöz S, Yanik J, Uçar S, Song C. Catalytic coprocessing of low-density polyethylene with VGO using metal supported on activated carbon. Energy Fuels 2002;16:1301–4. https://doi.org/10.1021/ef020064q.
[19] Vela FJ, Palos R, Bilbao J, Arandes JM, Gutiérrez A. Effect of co-feeding HDPE on the product distribution in the hydrocracking of VGO. Catal Today 2020;353:197–203. https://doi.org/10.1016/j.cattod.2019.07.010.
[20] Quitian A, Ancheyta J. Experimental methods for developing kinetic-models for hydrocracking reactions with slurry-phase catalyst using batch reactors. Energy Fuels 2016;30:4419–37. https://doi.org/10.1021/acs.energyfuels.5b01953.
[21] Bdwi EAS, Ali SA, Quddus MR, Al-Bogami SA, Razzak SA, Hossain MM. Kinetics of promotional effects of oil-soluble dispersed metal (Mo Co, and Fe) catalysts on slurry phase hydrocracking of vacuum gas oil. Energy Fuels 2017;31:3132–42. https://doi.org/10.1021/acs.energyfuels.6b03322.
[22] Ortega Garcia FJJ, Muñoz Arroyo JAA, Flores Sánchez P, Mar Juárez E, Dominguez Esquivel JMM. Hydrocracking kinetics of a heavy crude oil on a liquid catalyst. Energy Fuels 2017;31:6794–9. https://doi.org/10.1021/acs.energyfuels.7b00639.
[23] Till Z, Varga T, Szabó L, Chován T. Identification and observability of lumped kinetic models for vacuum gas oil hydrocracking. Energy Fuels 2017;31:12654–64. https://doi.org/10.1021/acs.energyfuels.7b02040.
[24] Till Z, Varga T, Sója J, Miskolczi N, Chován T. Reduction of lumped reaction networks based on global sensitivity analysis. Chem Eng J 2019;375. https://doi.org/10.1016/j.cej.2019.121920.
[25] Browning B, Pitault I, Couenne F, Jansen T, Lacroix M, Alvarez P, et al. Distributed lump kinetic modeling for slurry phase vacuum residue hydroconversion. Chem Eng J 2019;377:119811. https://doi.org/10.1016/j.cej.2018.08.197.
[26] Li M, Ren T, Sun Y. Analysis of reaction path and different lumped kinetic models for asphaltene hydrocracking. Fuel 2022;325:124840. https://doi.org/10.1016/j.fuel.2022.124840.
[27] Van de Vijver R, Devocht BR, Van Geem KM, Thybaut JW, Marin GB. Challenges and opportunities for molecule-based management of chemical processes. Curr Opin Chem Eng 2016;13:142–9. https://doi.org/10.1016/j.coche.2016.09.006.
[28] Becker PJ, Serrand N, Celse B, Guillaume D, Dulot H. Comparing hydrocracking models: continuous lumping vs. single events. Fuel 2016;165:306–15. https://doi.org/10.1016/j.fuel.2015.09.091.
[29] Félix G, Ancheyta J. Comparison of hydrocracking kinetic models based on SARA fractions obtained in slurry-phase reactor. Fuel 2019;241:495–505. https://doi.org/10.1016/j.fuel.2018.11.153.
[30] Félix G, Ancheyta J, Trejo F. Sensitivity analysis of kinetic parameters for heavy oil hydrocracking. Fuel 2019;241:836–44. https://doi.org/10.1016/j.fuel.2018.12.058.
[31] Félix G, Ancheyta J. Using separate kinetic models to predict liquid, gas, and coke yields in heavy oil hydrocracking. Ind Eng Chem Res 2019;58:7973–9. https://doi.org/10.1021/acs.iecr.9b00904.
[32] Félix G, Tirado A, Yuan C, Varfolomeev MA, Ancheyta J. Analysis of kinetic models for hydrocracking of heavy oils for in-situ and ex-situ applications. Fuel 2022;323:124322. https://doi.org/10.1016/j.fuel.2022.124322.
[33] Rodríguez E, Félix G, Ancheyta J, Trejo F. Modeling of hydrotreating catalyst deactivation for heavy oil hydrocarbons. Fuel 2018;225:118–33. https://doi.org/10.1016/j.fuel.2018.02.085.
[34] Bin Jumah A, Malekshahian M, Tedstone AA, Garforth AA. Kinetic modeling of hydrocracking of low-density polyethylene in a batch reactor. ACS Sustain Chem Eng 2021;9:16757–69. https://doi.org/10.1021/acssuschemeng.1c06231.
[35] Vela FJ, Palos R, Trueba D, Bilbao J, Arandes JM, Gutiérrez A. Different approaches to convert waste polyolefins into automotive fuels via hydrocracking with a NiW/HY catalyst. Fuel Process Technol 2021;220:106891. https://doi.org/10.1016/j.fuproc.2021.106891.
[36] Gutiérrez A, Arandes JM, Castaño P, Olazar M, Bilbao J. Preliminary studies on fuel production through LCO hydrocracking on noble-metal supported catalysts. Fuel 2012;94:504–15. https://doi.org/10.1016/j.fuel.2011.10.010.
[37] Vela FJ, Palos R, Bilbao J, Arandes JM, Gutiérrez A. Hydrogen pressure as a key parameter to control the quality of the naphtha produced in the hydrocracking of

an HDPE/VGO blend. Catalysts 2022;12:543. https://doi.org/10.3390/catal12050543.
[38] Al-Attas TA, Zahir MH, Ali SA, Al-Bogami SA, Malaibari Z, Razzak SA, et al. Novel (Co-, Ni)-p-*tert*-butylcalix[4]arenes as dispersed catalysts for heavy oil upgrading: synthesis, characterization, and performance evaluation. Energy Fuels 2019;33:561–73. https://doi.org/10.1021/acs.energyfuels.8b03619.
[39] Purón H, Arcelus-Arrillaga P, Chin KK, Pinilla JL, Fidalgo B, Millan M, et al. Kinetic analysis of vacuum residue hydrocracking in early reaction stages. Fuel 2014;117:408–14. https://doi.org/10.1016/j.fuel.2013.09.053.
[40] Faraji D, Sadighi S, Mazaheri H. Modeling and evaluating zeolite and amorphous based catalysts in vacuum gas oil hydrocracking process. Int J Chem React Eng 2018;16:1–14. https://doi.org/10.1515/ijcre-2017-0030.
[41] Al-Attas TA, Zahir MH, Ali SA, Al-Bogami SA, Malaibari Z, Razzak SA, et al. Kinetics of the synergy effects in heavy oil upgrading using novel Ni-p-tert-butylcalix[4]arene as a dispersed catalyst with a supported catalyst. Fuel Process Technol 2019;185:158–68. https://doi.org/10.1016/j.fuproc.2018.12.003.
[42] Lababidi HMS, AlHumaidan FS. Modeling the hydrocracking kinetics of atmospheric residue in hydrotreating processes by the continuous lumping approach. Energy Fuels 2011;25:1939–49. https://doi.org/10.1021/EF200153P.
[43] Elizalde I, Ancheyta J. Modeling catalyst deactivation during hydrocracking of atmospheric residue by using the continuous kinetic lumping model. Fuel Process Technol 2014;123:114–21. https://doi.org/10.1016/j.fuproc.2014.02.006.
[44] Ramdoss PKK, Tarrer ARR. High-temperature liquefaction of waste plastics. Fuel 1998;77:293–9. https://doi.org/10.1016/S0016-2361(97)00193-2.
[45] Sánchez S, Rodríguez MA, Ancheyta J. Kinetic model for moderate hydrocracking of heavy oils. Ind Eng Chem Res 2005;44:9409–13. https://doi.org/10.1021/ie050202.
[46] Al-Rashidy AH, Al-Attas TA, Ali SA, Al-Bogami SA, Razzak SA, Hossain MM. Hydrocracking of LVGO using dispersed catalysts derived from soluble precursors: performance evaluation and kinetics. Ind Eng Chem Res 2019;58:14709–18. https://doi.org/10.1021/acs.iecr.9b02658.
[47] Cordero-Lanzac T, Aguayo AT, Gayubo AG, Castaño P, Bilbao J. Simultaneous modeling of the kinetics for n-pentane cracking and the deactivation of a HZSM-5 based catalyst. Chem Eng J 2018;331:818–30. https://doi.org/10.1016/j.cej.2017.08.106.
[48] Cordero-Lanzac T, Aguayo AT, Castaño P, Bilbao J. Kinetics and reactor modeling of the conversion of n-pentane using HZSM-5 catalysts with different Si/Al ratios. React Chem Eng 2019;4:1922–34. https://doi.org/10.1039/c9re00222g.
[49] Palos R, Rodríguez E, Gutiérrez A, Bilbao J, Arandes JM. Kinetic modeling for the catalytic cracking of tires pyrolysis oil. Fuel 2022;309:122055. https://doi.org/10.1016/j.fuel.2021.122055.
[50] Angeles MJJ, Leyva C, Ancheyta J, Ramírez S. A review of experimental procedures for heavy oil hydrocracking with dispersed catalyst. Catal Today 2014;220–222:274–94. https://doi.org/10.1016/j.cattod.2013.08.016.
[51] Calderón CJ, Ancheyta J. Modeling of CSTR and SPR small-scale isothermal reactors for heavy oil hydrocracking and hydrotreating. Fuel 2018;216:852–60. https://doi.org/10.1016/j.fuel.2017.11.089.
[52] Sánchez S, Ancheyta J. Effect of pressure on the kinetics of moderate hydrocracking of Maya crude oil. Energy Fuels 2007;21:653–61. https://doi.org/10.1021/ef060525y.
[53] Sadighi S, Ahmad A, Masoudian SKK. Effect of lump partitioning on the accuracy of a commercial vacuum gas oil hydrocracking model. Int J Chem React Eng 2012;10:1–22. https://doi.org/10.1515/1542-6580.2616.
[54] Martínez J, Ancheyta J. Kinetic model for hydrocracking of heavy oil in a CSTR involving short term catalyst deactivation. Fuel 2012;100:193–9. https://doi.org/10.1016/j.fuel.2012.05.032.
[55] Asaee SDS, Vafajoo L, Khorasheh F. A new approach to estimate parameters of a lumped kinetic model for hydroconversion of heavy residue. Fuel 2014;134:343–53. https://doi.org/10.1016/j.fuel.2014.05.079.
[56] Manek E, Haydary J. Hydrocracking of vacuum residue with solid and dispersed phase catalyst: Modeling of sediment formation and hydrodesulfurization. Fuel Process Technol 2017;159:320–7. https://doi.org/10.1016/j.fuproc.2017.02.003.
[57] Abid MF, Ahmed SM, Hassan HH, Ali SM. Modeling and kinetic study of an ebullated bed reactor in the H-Oil process. Arab J Sci Eng 2018;43:5733–43. https://doi.org/10.1007/s13369-017-2958-4.
[58] Pérez-Uriarte P, Ateka A, Aguayo AT, Gayubo AG, Bilbao J. Kinetic model for the reaction of DME to olefins over a HZSM-5 zeolite catalyst. Chem Eng J 2016;302:801–10. https://doi.org/10.1016/J.CEJ.2016.05.096.
[59] Gayubo AG, Alonso A, Valle B, Aguayo AT, Olazar M, Bilbao J. Kinetic modelling for the transformation of bioethanol into olefins on a hydrothermally stable Ni–HZSM-5 catalyst considering the deactivation by coke. Chem Eng J 2011;167:262–77. https://doi.org/10.1016/J.CEJ.2010.12.058.
[60] Ancheyta J, Sotelo-Boyás R. Estimation of kinetic constants of a five-lump model for fluid catalytic cracking process using simpler sub-models. Energy Fuels 2000;14:1226–31. https://doi.org/10.1021/ef000097a.
[61] Monzón A, Romeo E, Borgna A. Relationship between the kinetic parameters of different catalyst deactivation models. Chem Eng J 2003;94:19–28. https://doi.org/10.1016/S1385-8947(03)00002-0.
[62] Morales-Blancas M, Mederos-Nieto FS, Elizalde I, Felipe Sánchez-Minero J, Trejo-Zárraga F. Discrete lumping kinetic models for hydrodesulfuration and hydrocracking of a mixture of FCC feedstock and light gasoil. Chem Pap 2022;1:1–7. https://doi.org/10.1007/s11696-022-02219-8.
[63] Huang T, Liu B, Wang Z, Guo X. Kinetic model for hydrocracking of Iranian heavy crude with dispersed catalysts in slurry-phase. Pet Sci Technol 2017;35:1846–51. https://doi.org/10.1080/10916466.2017.1367801.
[64] Menegassi R, Almeida D, Guirardello R. Hydroconversion kinetics of Marlim vacuum residue 2005;109:104–11. 10.1016/j.cattod.2005.08.021.
[65] Hassanzadeh H, Abedi J. Modelling and parameter estimation of ultra-dispersed in situ catalytic upgrading experiments in a batch reactor. Fuel 2010;89:2822–8. https://doi.org/10.1016/J.FUEL.2010.02.012.
[66] Pham HH, Kim KH, Go KS, Nho NS, Kim W, Kwon EH, et al. Hydrocracking and hydrotreating reaction kinetics of heavy oil in CSTR using a dispersed catalyst. J Pet Sci Eng 2021;197:107997. https://doi.org/10.1016/j.petrol.2020.107997.
[67] Fals J, García JR, Falco M, Sedran U. Coke from SARA fractions in VGO. Impact on Y zeolite acidity and physical properties. Fuel 2018;225:26–34. https://doi.org/10.1016/j.fuel.2018.02.180.